

Plasmon localization and giant fields in holographic metasurface for SERS sensors

Andrey K. Sarychev,^{*} Andrey Ivanov, Andrey N. Lagarkov, Ilya Ryzhikov, and Konstantin Afanasev
*Institute for Theoretical and Applied Electrodynamics,
 Russian Academy of Sciences, 125412, Moscow, Russia*

Igor Bykov
*Institute for Theoretical and Applied Electrodynamics,
 Russian Academy of Sciences, 125412, Moscow, Russia;
 Laboratory of Nano-Bioengineering, National Research Nuclear University MEPhI
 (Moscow Engineering Physics Institute), 31 Kashirskoe shosse, Moscow 115521, Russia*

Grégory Barbillon
*EPF-Ecole d'Ingénieurs,
 3 bis rue Lakanal, 92330 Sceaux, France*

Nikita Bakholdin and Mikhail Mikhailov
*National Research University "Moscow Power Engineering Institute",
 Krasnokazarmennaya 14, Moscow 111250, Russia*

Alexander Smyk and Alexander Shurygin
James River Branch llc, 8, Tvardovsky st., Strogino Industrial Park Moscow 123458, Russia

Alexander Shalygin
*Lomonosov Moscow State University, Faculty of Physics,
 GSP-1, 1-2 Leninskiye Gory, Moscow 119991, Russia
 (Dated: January 20, 2022)*

We present SERS-active metal holographic metasurfaces fabricated from metal periodical nanograting deposited on a dielectric substrate. The metasurface consists of a modulated dielectric, which is covered by a thin silver layer. The metasurface operates as an open plasmon resonator. The theory of plasmons excited in the open resonator formed by a metal nanograting is presented. The large local electromagnetic field is predicted for optical frequencies. The excitation of plasmons is experimentally demonstrated in the metasurface designed on a 4-inch Si wafer. The enhancement of the local electric field results in surface-enhanced Raman scattering (SERS). To investigate the SERS effect, the metasurfaces are covered by molecules of 4-mercaptophenylboronic acid, which form covalent bonds with the silver nanolayer and serve as a proof-of-concept. Finally, we obtain a detection limit of 230 nM for molecules of 4-mercaptophenylboronic acid.

I. INTRODUCTION

The design of a nanoresonator with a high enhancement of the local electric field is an important point for the application to the surface-enhanced Raman scattering (SERS) and other plasmon-enhanced spectroscopies. It is important to increase the selectivity and sensitivity of the biological and chemical sensing [1–4]. The novel fabrication techniques allow to produce sophisticated resonant substrates with the controllable shape and arrangement of the resonators [5]. These techniques include focused ion-beam lithography [6], electron-beam lithography [7–10], X-ray, UV, plasmonic cavity lens (PCL) and interference lithographs [11–16], nanoimprint Lithography (NIL) [17–19], nanosphere lithography (NSL) [20–23], laser-induced transfer metal nanodroplets [24]. Some

of them allow to realize reproducible SERS substrates with a lower cost and a larger active surface area, for example, interference lithography. In references [11, 15], the gold and hybrid gold-silver nanodisk array fabricated via X-ray interference lithography is proposed. The effectiveness of the structures has been proven by the detection of a low concentration of Rhodamine 6G (R6G) molecules via SERS with enhancement factor $10^5 - 10^6$. The authors admitted high sensitivity, reproducibility and stability of such structures. In reference [16], silver nanohole arrays are proposed. A photoresist layer sandwiched with two Ag layers increases Q-factor of nanoresonators and the sensitivity. The SERS substrates exhibited enhancement factors (EFs) of 10^7 that are capable of monolayer detection of R6G molecules. It should be noted that optically mirror underlayer, which is designed to increase Q-factor, was theoretically predicted and experimentally investigated by the authors [4, 25–27]. Theoretical predictions and experimental studies have shown giant electromagnetic field fluctuations in the

^{*} sarychev_andrey@yahoo.com

case of almost touched plasmonic nanoparticles [28–36]. It was shown that plasmonic nanocavities confining the light to unprecedentedly small volumes, support multiple types of modes. Different nature of these modes leads to the mode beating within the nanocavity and the Rabi oscillations, which alter the spatio-temporal dynamics of the hybrid system [37]. By intermixing plasmonic excitation in nanoparticle arrays with excitons in a WS_2 monolayer inside a resonant metal microcavity, the hierarchical system was fabricated with the collective microcavity-plasmon-exciton Rabi splitting exceeding 0.5 eV at room temperature. Gap-surface plasmon metasurfaces, which consist of a subwavelength thin dielectric spacer sandwiched between an optically thick film of metal and arrays of metal subwavelength elements arranged in a strictly or quasiperiodic fashion, have a possibility to fully control the amplitude, phase, and polarization of the reflected light [30, 38].

Open resonators can very effectively accumulate the electromagnetic energy (see, e.g., [39]). In the optical frequency range, a corrugated metal surface can operate as an open resonator and generate large local electric field [40–43]. The method of the transformation optics was developed to calculate optical properties of metamaterials [44, 45]. This method was used to investigate reflection from the metal gratings in recent papers [46–49]. The authors develop an original conformal mapping that transforms one-side metal grating into rectangular metal slab that optical properties can be found. For instance, to calculate the reflection of an electromagnetic wave, the metal grating is replaced by thin plane metal film. The developed method was used to theoretically investigate broadband THz absorption in graphene metasurfaces [50], optical properties of singular metal surfaces [48, 51], non-local effects [52], and calculating of the energy loss of an electron flying over the metal modulation [53].

Strong motivation for the investigation of open plasmon resonators is the SERS effect, which is mainly due to the local electric field enhancement. The SERS effect enables identification of trace molecules captured by the corrugated metal surface. The SERS is extremely important for medical diagnostics, for instance, for cancer detection, imaging and therapy, drug delivery, quantitative control of biomarkers including glycated proteins and cardiovascular biomarkers [55–60].

In this paper, we present the analytical theory as well as experimental observation of the plasmons excited in open resonators formed by a periodic metal grating. The resonance condition of the open plasmon resonator is found, when it is possible to achieve large electromagnetic field enhancement both inside and in the vicinity of the plasmonic grating. This will increase the sensitivity of SERS-probing and other surface-enhanced spectroscopies. The modulated silver film is produced by four-ray holographic process and its optical properties are measured. The silver metasurfaces are covered by molecules of 4-mercaptophenylboronic acid to investigate

the SERS in metasurfaces made by optical interference lithography. Holographic SERS substrates are easy-made and low-cost for mass production, and they have allowed to achieve a detection limit of 230 nM for molecules of 4-mercaptophenylboronic acid (4-mPBA).

II. ANALYTICAL THEORY

We consider periodic metal gratings that support localized plasmons whose size can reach few hundred nanometers. The metal gratings with two-side modulation efficiently concentrate and store electromagnetic energy. The local electric field is resonantly enhanced. The localized plasmons are analytically calculated using a quasistatic approximation for the nanogratings whose dimensions (thickness and modulation) are much smaller than the wavelength λ .

A. Plasmon resonance in metal nanotube

To understand how the metasurface works, let us solve a simple two-dimensional plasmonic system, which is interesting by itself since it has a non-trivial analytical solution. We investigate the plasmon resonance and the corresponding electromagnetic field enhancement in the metal nanotube that radius and thickness are much smaller than the wavelength λ . The length of the metal nanotube is much larger than the radius. The vector of the external electric field lies in the $u-v$ plane perpendicular to tube axis. Since the transversal dimensions of the nanotube is much smaller than the wavelength the problem is reduced to the two dimensional problem of the excitation of the infinite metal nanotube by the $E = \{E_u, E_v\}$ electric field, which is normal to the tube axis. For further simplification, we neglect retardation effects and use the quasistatic approximation when the plasmonic electric field is found from the electric potential $\varphi(u, v)$. The two dimensional problem can be solved by considering potential, electric field, and charge in $u-v$ plane using theory of functions of a complex variable. All the distances are measured in terms of the internal radius of the nanotube.

Thus, we calculate the plasmon resonance and the field enhancement in a metal ring with radius r_0 , the thickness d_0 , and the metal permittivity ε_m , shown in Fig. 1 by red color. To find the field in the ring, we introduce the Descartes coordinates u, v , and the complex variable $w = u + iv$. The ring has the center at $u = v = 0$. It is surrounded by a dielectric host ε_d , blue color in Fig. 1; the medium inside the ring has permittivity ε_1 (light green in Fig. 1). The electromagnetic field is excited by the point "magnetic" monopole, which generates in the surrounding space the electric potential $\varphi_s = \Re\varphi_{sing}$, where the complex potential equals to

$$\varphi_{sing} = iE_0 \log(w - x_0), \quad (1)$$

where $u = x_0$ and $v = 0$ are coordinates of the monopole (horizontal blue line in Fig. 1). The exact nature of the monopole is irrelevant for the material presented below.

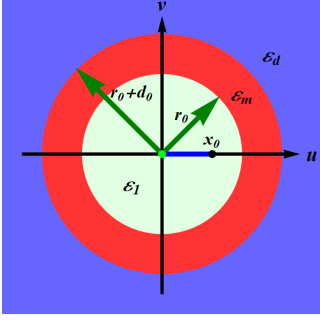


FIG. 1. Metal disk in plane $u-v$ with permittivity of internal space ε_1 , metal permittivity ε_m , permittivity of outer space ε_d , and a "magnetic" monopole placed at $u = x_0, v = 0$.

The monopole oscillates with the frequency ω , and the amplitude E_0 is assumed, for simplicity, to be positive $E_0 > 0$. Recall the quasistatic approximation is used, when the field retardation is neglected. Then, the electric potential φ is the solution of the Laplace equation $\Delta\varphi = 0$ that holds in all the space but the monopole center. As usual in two-dimensional (2D) problem, a complex electric field is introduced $\tilde{E} = E_u - iE_v = -d\varphi/dw$. The field is expanded into radial $E_r = \Re(w\tilde{E})/r \equiv (E_u u + E_v v)/r$ and angular $E_\phi = -\Im(w\tilde{E})/r \equiv (-E_u v + E_v u)/r$ components, where $r = |w| = \sqrt{u^2 + v^2}$. The electric charges, induced by the monopole, are uniformly distributed in the metal ring when the monopole is placed in the center. Therefore, angular component of the electric field remains to be the same inside and outside the ring. For the central monopole ($x_0 = 0$) with amplitude $E_0 > 0$, the interior electric field $E^{(i)}(r < 1)$, the field $E^{(m)}(1 \leq r \leq 1 + d_0)$ in the ring, and the outer field $E^{(e)}(r > 1 + d_0)$ have only angular components. The interior, ring, and outer fields are all equal to $E_r^{(i)} = E_r^{(m)} = E_r^{(e)} = 0$ and $E_\phi^{(i)} = E_\phi^{(m)} = E_\phi^{(e)} = E_0/r$. As we see, the central monopole does not excite the plasmon regardless of the value of the metal permittivity ε_m .

Yet, this is an unstable solution. Plasmons are excited when monopole is shifted from the center. Suppose that the monopole is set at $u = x_0 < 1, v = 0$. The interior complex potential equals to

$$\begin{aligned} \varphi^{(i)}(w) &= \varphi_{sing}(w) + \varphi_{reg}^{(i)}(w) = \\ iE_0[\log(w - x_0) + \varphi_{reg}^{(i)}(w)], \quad r \leq 1 \end{aligned} \quad (2)$$

where $\varphi_{reg}^{(i)}(w)$ is a regular part of the interior potential that can be expressed in series of w that only contains positive powers. To simplify the consideration, we neglect for a moment the loss in the metal assuming that permittivity ε_m has zero imaginary part. The complex interior field equals to

$$\begin{aligned} \tilde{E}^{(i)}(w) &= -\frac{d\varphi(w)}{dw} = \\ -iE_0 \left[\frac{1}{w - x_0} + \sum_{n=1}^{\infty} A_n w^{n-1} x_0^n \right], \quad r \leq 1, \end{aligned} \quad (3)$$

where $0 < x_0 < 1$ and it is still assumed that E_0 is real. The first term in Eq. (3) is expanded in series of $(x_0/w)^n$ for $x_0 < |w| < 1$, and we obtain

$$\begin{aligned} \tilde{E}^{(i)}(w) &= -iE_0 [w^{-1} + \\ \sum_{n=1}^{\infty} x_0^n (A_n w^{n-1} + w^{-n-1})], \quad r \leq 1 \end{aligned} \quad (4)$$

where coefficients A_n take real values. The electric field in the metal ring is expanded in Laurent series:

$$\begin{aligned} \tilde{E}^{(m)}(w) &= -iE_0 [w^{-1} + \\ \sum_{n=1}^{\infty} x_0^n (B_n w^{-n-1} + C_n w^{n-1})], \quad 1 < r < 1 + d \end{aligned} \quad (5)$$

and the outer complex field decreases when the radius $r \equiv |w|$ goes to infinity:

$$\begin{aligned} \tilde{E}^{(e)}(w) &= -iE_0 [w^{-1} + \sum_{n=1}^{\infty} x_0^n D_n w^{-n-1}], \quad (6) \\ r &\geq 1 + d \end{aligned}$$

These complex fields can be split in radial and angular parts, namely,

$$E = \{E_r, E_\phi\} = \left\{ \Re \left[\tilde{E} \frac{w}{r} \right], -\Im \left[\tilde{E} \frac{w}{r} \right] \right\}.$$

For example, the internal field $E^{(i)}$ has the following radial and angular components

$$\{E_r^{(i)}, E_\phi^{(i)}\} = E_0 \{0, r^{-1}\} + E_0 \sum_{n=1}^{\infty} r^{-n-1} x_0^n \{ (A_n r^{2n} - 1) \sin(n\phi), (A_n r^{2n} + 1) \cos(n\phi) \}, \quad r \leq 1 \quad (7)$$

The $\{E_r, E_\phi\}$ expansion of the internal $E^{(i)}$, ring $E^{(m)}$, and outer $E^{(e)}$ fields holds even if the coefficients A_n, B_n, C_n, D_n are complex values. The coefficients ascribe complex values since the metal permittivity has

imaginary part $\varepsilon_m = \varepsilon_{m1} + i\varepsilon_{m2}$ due to ohmic loss.

The important value of the intensity $I^{(i)} = |E^{(i)}|^2 / |E_0|^2$ of the internal field, which is averaged over the internal surface of the metal ring, ($|w| \equiv r = 1$) equals to

$$\langle I^{(i)} \rangle = \frac{1}{2\pi} \int_0^{2\pi} |E^{(i)}(r=1, \phi)|^2 d\phi = 1 + \frac{1}{2} \sum_{n=1}^{\infty} x_0^{2n} (|A_n|^2 + 1) \equiv 1 + \sum_{n=1}^{\infty} I_n \quad (8)$$

where the coefficients A_n are given below by Eq. (12). The coefficients A_n, B_n, C_n, D_n in Eqs. (3) – (8) are found from the boundary conditions for the electric fields at internal surface ($|w| = 1$) and outer surface ($|w| = 1 + d_0$) of the ring:

$$\varepsilon_1 E_r^{(i)} = \varepsilon_m E_r^{(m)}, \quad E_\phi^{(i)} = E_\phi^{(m)}, \quad |w| = 1, \quad (9)$$

$$\varepsilon_m E_r^{(m)} = \varepsilon_d E_r^{(e)}, \quad E_\phi^{(m)} = E_\phi^{(e)}, \quad |w| = 1 + d_0 \quad (10)$$

where $\varepsilon_1, \varepsilon_m$ and ε_d are the permittivities of the internal space ($r \leq 1$), metal ring ($1 < r < 1 + d_0$) and the outer space ($r \geq 1 + d_0$), respectively. We substitute the series (3) – (7) in the above boundary equations and equate the coefficients at the same power of x_0 . It is easy to verify that the coefficients at x_0^n in all series (3)-(7) have the same angular dependence. Thus, the following basic equations are obtained:

$$\begin{aligned} A_n + 1 &= B_n + C_n, \quad \varepsilon_1 (A_n - 1) = \varepsilon_m (C_n - B_n), \\ B_n + C_n d_{2n} &= D_n, \quad \varepsilon_m (B_n - C_n d_{2n}) = \varepsilon_d D_n \end{aligned} \quad (11)$$

where $d_{2n} = (1 + d_0)^{2n}$. Solution of these equations gives the coefficients

$$\begin{aligned} A_n &= \frac{d_{2n}(\varepsilon_1 - \varepsilon_m)(\varepsilon_d + \varepsilon_m) - (\varepsilon_m + \varepsilon_1)(\varepsilon_d - \varepsilon_m)}{\det_n}, \quad (12) \\ B_n &= \frac{2d_{2n}(\varepsilon_d + \varepsilon_m)}{\det_n}, \quad C_n = \frac{2(\varepsilon_m - \varepsilon_d)}{\det_n}, \quad D_n = \frac{4d_{2n}\varepsilon_m}{\det_n} \end{aligned}$$

that completely determine the electric field inside, in, and out of the plasmonic ring. The determinant \det_n of equations Eq. (11) that is the denominator in Eqs. (12) equals to

$$\det_n = d_{2n} (\varepsilon_m + \varepsilon_1) (\varepsilon_m + \varepsilon_d) + (\varepsilon_1 - \varepsilon_m) (\varepsilon_m - \varepsilon_d) \quad (13)$$

Zeroing of the determinant $\det_n = 0$ gives the condition for the n -th resonance exciting in the plasmonic ring. For the given permittivities of the metal ring ε_m and outer space ε_d , the ring resonates when its thickness takes the following values:

$$\begin{aligned} d_{0res,n} &= r_0 \Re \left[\left(\frac{(\varepsilon_1 - \varepsilon_m)(\varepsilon_d - \varepsilon_m)}{(\varepsilon_m + \varepsilon_1)(\varepsilon_d + \varepsilon_m)} \right)^{\frac{1}{2n}} - 1 \right] \simeq \\ &r_0 \left[\left(\frac{(\varepsilon_1 - \varepsilon_{m1})(\varepsilon_d - \varepsilon_{m1})}{(\varepsilon_{m1} + \varepsilon_1)(\varepsilon_d + \varepsilon_{m1})} \right)^{\frac{1}{2n}} - 1 \right] \end{aligned} \quad (14)$$

where we restore natural dimensions and insert the radius r_0 of the ring. $n = 1, 2, 3, \dots$ is the resonance number, i.e., $2n$ is the number of nodes in the ring field $E^{(m)}$ (see Fig. 2). In transition to the second estimation in Eq. (14), it is taken into account that the real part $\varepsilon_{m1} = \Re[\varepsilon_m]$ of the metal permittivity is much larger in absolute value than the imaginary part $\varepsilon_{m2} = \Im[\varepsilon_m] \ll |\varepsilon_{m1}|$ for the "good" optical metals like silver or gold. We obtain an

expected result: the ring resonates if and only if the real part of the metal permittivity is negative. For the red and infrared parts of the optical spectrum, the real part ε_{m1} of the metal permittivity is negative and large in absolute value. Then, the dispersion equation Eq. (14) simplifies to

$$d_{0res,n} \simeq r_0 \frac{\varepsilon_d + \varepsilon_1}{n|\varepsilon_m|} \quad (15)$$

where r_0 is the radius of the ring. We obtain that the resonance thickness of the metal layer is inverse proportional to the absolute value of the metal permittivity.

The dimensionless intensity $\langle I^{(i)} \rangle$ of the resonance electric field averaged over the internal surface of the ring with thickness $d_{0res,n}$ estimates as $\langle I^{(i)}(d = d_{0res,n}) \rangle = I_{0max,n} \simeq I_n$ from Eq. (8):

$$I_{0max,n} \simeq 2 \left[\frac{\varepsilon_1 \varepsilon_{m1} (\varepsilon_d^2 - \varepsilon_{m1}^2)}{\varepsilon_{m2} (\varepsilon_d + \varepsilon_1) (\varepsilon_{m1}^2 - \varepsilon_1 \varepsilon_d)} \right]^2 \left(\frac{x_0}{r_0} \right)^{2n} \quad (16)$$

where $\varepsilon_{m1} = \Re \varepsilon_m$ and $\varepsilon_{m2} = \Im \varepsilon_m$. Excitation of various resonances in the silver ring is illustrated in Fig. 2 for the wavelength $\lambda = 785 \text{ nm}$. The silver permittivity for this wavelength is $\varepsilon_m \simeq -30 + 0.4i$ [61], and the permittivity of the outer space is chosen to be $\varepsilon_d = 2$, which corresponds to the permittivity of the photoresist in our experiments. The first three resonances are displayed in Figure 2. The electric field in a metal ring has two, four and six nodes for the first, second and third resonances, respectively. Note the first dipole resonance electric field, shown in Figure 2a, fills all the internal space of the ring. This result corresponds to the electric field distribution in the metal cylinder excited by an uniform external electric field [62]. A plasmon excited in

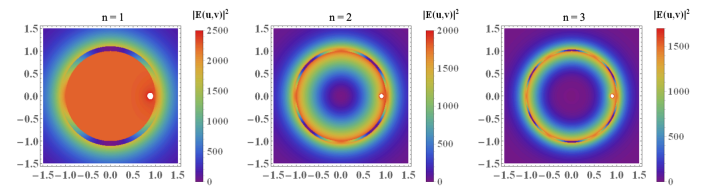


FIG. 2. Electric field in the silver ring for the plasmon resonances $n = 1, 2, 3$ at an excitation wavelength of $\lambda = 785 \text{ nm}$. Silver permittivity is $\varepsilon_m \approx -30 + 0.4i$, internal permittivity $\varepsilon_1 = 1$, outer permittivity $\varepsilon_d = 2$, ring thickness $d_{0res,n} = 0.11, 0.052, 0.034$, all dimensions are normalized to the ring radius r_0 . The white spot corresponds to the monopole, which is placed at $u = x_0 = 0.9, v = 0$.

a metal tube can be experimentally investigated. Suppose that the nanochannels with radius r_0 are formed in a dielectric material. Nanochannels can be produced,

for instance, in the silicon by the electrochemical etching (see [63] and reference therein). The surface of the nanochannels is covered by a silver layer with the thickness $d_{res,1} \simeq r_0(\varepsilon_d + 1)/(|\varepsilon_m|)$ given by Eq. (15). Suppose further that the Raman-active analyte is injected in these channels. Then, the Raman signal from the molecules in the nanochannels is much enhanced since the scattering is incoherent and the Raman intensities are summed up. The Raman enhancement factor (SERS) estimates as $G \sim I_{max,n}^2$ (see, e.g., [64]), where $I_{max,n} \gg 1$ is given by Eq. (16) and the parameter $x_0 \sim r_0$. For the typical Raman spectroscopy wavelength of $\lambda = 785 \text{ nm}$, the silver permittivity is about $\varepsilon_m \simeq -30 + 0.4i$ and the enhancement factor estimates as $G \sim (\varepsilon_{m1}/\varepsilon_{m2})^4 \sim 10^7$. This esteem holds for any argument of the complex amplitude E_0 . For instance, in the case $E_0 = -2iQ$, $Q > 0$ the monopole potential (1) is the potential of the usual electric charge, which density equals to $Q\delta(u - x_0)\delta(v)$. Any other field sources such as a dipole or quadrupole, can be combined from electric monopoles.

B. Giant electric field in metal grating

We consider a modulated metal film. The metal grating is placed at the plane $X = 0$. The electromagnetic wave propagates along X -axis being "y"-polarized, i.e., $E \sim \{0, E_0, 0\} \exp(ikX)$, where $k = \omega/c$ is the wavevector. The wave impinges on the front surface of the grating, where the plasmon is excited due to the modulation (see Figure 3a). In this section devoted to the analytical consideration, we assume that the film modulation h as well as its period L are much smaller than the wavelength $\lambda = 2\pi/k$. In this case, we can approximate $E \sim \{0, E_0, 0\} \exp(ikX) \simeq \{0, E_0, 0\}$ that is the plasmon grating is excited by uniform field E_0 , which is y -directed and oscillates with frequency ω . It is convenient to introduce the complex variable $Z = X + iY$. We use the quasistatic approach, therefore, the incident field is described by the complex potential $\varphi(Z) = iZE_0$, where we assume that the field E_0 takes real values. Then, $E_x = -\Re[d\varphi(Z)/dZ] = 0$, $E_y = \Im[d\varphi(Z)/dZ] = E_0$ (see Fig.3). It is convenient to shift from the real coordinates X and Y to the dimensionless coordinates x and y that are defined by using the period of the film modulation L , namely, $x = 2\pi X/L$ and $y = 2\pi Y/L$. That is the periodically modulated metal film has "natural" period of 2π being considered in x and y frame as shown in Figure 3a. Recall we use the quasistatic approximation, since the amplitude of metal modulation is assumed to be much smaller than the wavelength of the incident light. The potential of the local electric field does not change after re-scaling of the coordinates, since there is no characteristic length in the Laplace equation:

$$\varphi(z) = izE_0, \quad (17)$$

where $z = x + iy$. The shape of the modulated metal is chosen in such way that the front surface $\{x_f, y_f\}$ of

the modulated metal film (left red surface in Fig. 3a) is given by the parametric equation, which it is convenient to write in a complex form

$$z^{(f)}(\phi) = x^{(f)}(\phi) + iy^{(f)}(\phi) = \log[\exp(i\phi) - x_0] \quad (18)$$

where the parameter x_0 is in the interval $0 < x_0 < 1$, the variable ϕ changes in the limits $-\infty < \phi < \infty$; the logarithm is the full analytical function defined in all Riemann surfaces so that y also varies within the limits of $-\infty < y < \infty$. The back surface $x_b(\phi) > x_f(\phi)$ of the metal film (right red surface in Fig. 3a) is given by the parametric equation:

$$z^{(b)}(\phi) = x^{(b)}(\phi) + iy^{(b)}(\phi) = \log[(1 + d_0) \exp(i\phi) - x_0] \quad (19)$$

where the parameter ϕ still changes in the limits $-\infty < \phi < \infty$. The shape of the metal film is fully defined by its period L the amplitude of the modulation $h = (x_{max}^{(f)} - x_{min}^{(f)}) \frac{L}{2\pi}$ and the largest film thickness $d = (x_{min}^{(b)} - x_{min}^{(f)}) \frac{L}{2\pi}$. The parameters d_0 and x_0 in the Eqs. (18) and (19) are expressed in terms of the film modulation h and the film thickness d , namely,

$$x_0 = \tanh\left(\frac{h_1}{2}\right), \quad d_0 = 2 \frac{\exp(d_1) - 1}{\exp(h_1) + 1} \quad (20)$$

where $h_1 = h(\frac{2\pi}{L})$ and $d_1 = d(\frac{2\pi}{L})$. Therefore, the period L , the modulation h , and thickness d completely determine the shape of the modulated metal film indeed. Note that the film defined by Eqs. (19) and (18) mimics a metal film obtained, for example, by the metal evaporation on the modulated dielectric substrate. During the deposition process, the metal concentrates on tops of the film (see Fig. 3a and 7). To find the optical electric field in and around a modulated metal film, illuminated by the incident light, we use new coordinates u and v that convenient to introduce in the complex form:

$$w = u + iv = \exp(z) + x_0, \quad (21)$$

where $z = x + iy$. In the transition from x, y frame to u, v frame, the whole metal film transforms to the ring $1 \leq |w| \leq 1 + d_0$. The front and back surfaces of the grating are transformed to the internal $|w| = 1$ and outer $|w| = 1 + d_0$ surface of the ring. All the space in front of the grating (left from the grating in Fig. 3a) transforms in the space inside the ring $|w| < 1$ in Fig. 1a, the space behind the grating (right from the grating in Fig. 3a) transforms into outer space of the ring $|w| > 1 + d_0$. That is the metal film in Fig. 3a is rolled into the metal tube in Fig. 1. The approach is similar to the map used in references [30, 46]. The electric potential given by Eq. (17) transforms in $\{u, v\}$ frame to the potential φ_{sing} in Eq. (1). Therefore, the complex electric potential $\varphi(z)$ for a modulated metal film equals to $\varphi(w(z))$, where $\varphi(w)$ is the potential, which is found in the previous subsection for the metal ring. The complex electric field inside and

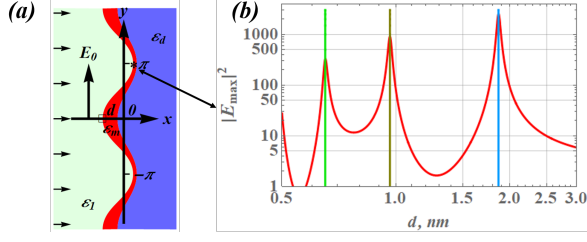


FIG. 3. (a) The design of plasmonic grating based on a metal film with a permittivity ε_m deposited on the modulated dielectric substrate (shown in blue) with a permittivity ε_d , metal film has thickness d , "y"-polarized light is incident from left; star "*" denotes the point with coordinates $x = x_{max}^{(f)}$ and $y = \pi$, where surface electric field has maximum; small open square "□" denotes the point with coordinates $x = x_{min}^{(f)}$ and $y = 0$, where surface electric field has minimum, the film modulation $h = (x_{max}^{(f)} - x_{min}^{(f)}) (L/2\pi)$. (b) Intensity of local electric field at surface of silver film, which is modulated with period L ; the field is shown in the point $X_{max} = x_{max}^{(f)} (L/2\pi)$ and $Y_{max} = \pi (L/2\pi)$ [star "*" in (a)] as function of the film thickness d , where the period is equal to $L = 50 \text{ nm}$, amplitude of the modulation is equal to $h = 11 \text{ nm}$, silver permittivity equals to $\varepsilon_m \approx -30 + 0.4i$ at 785 nm , permittivity of dielectric substrate equals to $\varepsilon_d = 2$, permittivity of front medium $\varepsilon_1 = 1$. Vertical color lines correspond to plasmon resonances given by Eq. (23).

around the modulated metal film is obtained from the following equation $\tilde{E}(z) = E_x - iE_y = -d\varphi(w(z))/dz = [-d\varphi(w)/dw][dw/dz] = [dw/dz]\tilde{E}(w)$, where the complex field $\tilde{E}(w)$ is given by Eqs. (3) – (7) and (12). The equation for the electric field E_x, E_y can be rewritten in the matrix form as follows:

$$\begin{bmatrix} E_x(x, y) \\ E_y(x, y) \end{bmatrix} = \begin{bmatrix} r - \frac{ux_0}{r} & \frac{vx_0}{r} \\ -\frac{vx_0}{r} & r - \frac{ux_0}{r} \end{bmatrix} \begin{bmatrix} E_r(u, v) \\ E_\phi(u, v) \end{bmatrix}, \quad (22)$$

where $\{E_x, E_y\}$ is the field in the metal film (see Figure 3a), $\{E_r, E_\phi\}$ are radial and angular components of the

field are given by Eq. (7), which is found for the plasmon resonance in the metal nanoring (see Figure 2), $r \equiv |w| = \sqrt{u^2 + v^2}$ is the radius in $\{u, v\}$ frame. The values of $u = \exp(x) \cos(y) + x_0$ and $v = \exp(x) \sin(y)$ are obtained from Eq. (21).

Below, we suppose that $E_0 = 1$ and measure all fields in terms of the applied field. The local electric field at the modulated metal surface in the point with coordinates

$$X_{max} = (L/2\pi)x_{max}^{(f)} = (L/2\pi)\log(1 + x_0), \\ Y_{max} = L/2 + mL \quad (m = 0, \pm 1, \pm 2, \dots)$$

of the modulated silver film is shown in Figure 3b as a function of the film thickness d . The wavelength of the incident light is $\lambda = 785 \text{ nm}$. The film is deposited on the dielectric with permittivity ε_d , and the permittivity of the front medium $\varepsilon_1 = 1$. The surface electric field is much enhanced for the film thickness corresponding to the excitation of plasmon resonances. The resonance thickness $d_{res,n}$ is obtained from Eqs. (14) and (20):

$$d_{res} = \frac{L}{2\pi} \log \left[\frac{\left(\frac{(\varepsilon_1 - \varepsilon_{m1})(\varepsilon_d - \varepsilon_{m1})}{(\varepsilon_1 + \varepsilon_{m1})(\varepsilon_d + \varepsilon_{m1})} \right)^{\frac{1}{2n}} - \tanh \frac{h_1}{2}}{1 - \tanh \frac{h_1}{2}} \right] \quad (23)$$

where L is the period and $h_1 = h(2\pi/L)$ is the dimensionless film modulation. The resonances are indicated by vertical lines in Figures 3b and 5a. The distributions of the local electric field for the three resonances are displayed in Figure 4. The local electric field is much enhanced and exceeds the incident field E_0 by two-three orders of magnitude. The enhanced field spreads over the grating achieving its maxima in the depressions of the front surface. The amplitude of the maximum field in the point with coordinates X_{max}, Y_{max} at the front surface of the metal film (star "*" in Fig. 3a) is given by the following equation obtained from Eq. (7) by substitution there $r = 1$ and $f = \pi$ and multiplying the result by matrix (22)

$$E_x(X_{max}, Y_{max}) = E_0(1 - x_0) \left[\frac{1}{1+x_0} + \sum_{n=1}^{\infty} (-x_0)^n \frac{(\varepsilon_1 + \varepsilon_m)(\varepsilon_m - \varepsilon_d) + (d_0 + 1)^{2n}(\varepsilon_1 - \varepsilon_m)(\varepsilon_d + \varepsilon_m)}{(\varepsilon_1 - \varepsilon_m)(\varepsilon_m - \varepsilon_d) + (d_0 + 1)^{2n}(\varepsilon_1 + \varepsilon_m)(\varepsilon_d + \varepsilon_m)} \right], \\ E_y(X_{max}, Y_{max}) = 0 \quad (24)$$

where the parameters x_0 and d_0 are given by Eqs. (20). The important characteristic is the amplitude of the resonance field averaged over the surface of the metal film, which has resonance thickness $d_{res,n}$ given by Eq. (23). The amplitude is still given by Eq. (16), where the ratio x_0/r_0 is replaced by $\tanh \frac{h_1}{2}$. For the practically important case $|\varepsilon_m| \gg \varepsilon_d$, the averaged intensity at the n -th

resonance is estimated as follows:

$$I_{max,n} \sim \left[\frac{\varepsilon_1 \varepsilon_{m1}}{\varepsilon_{m2}(\varepsilon_d + \varepsilon_1)} \tanh^n \frac{h_1}{2} \right]^2 \quad (25)$$

where $h_1 = h(\frac{2\pi}{L})$ and we skip numerical coefficient on the order one. The analytical results are compared with results of computer simulations. Computer simulations are performed for the electromagnetic field distribution in a weakly profiled silver film deposited on a photore-sist. The dimensions of the computer model are the

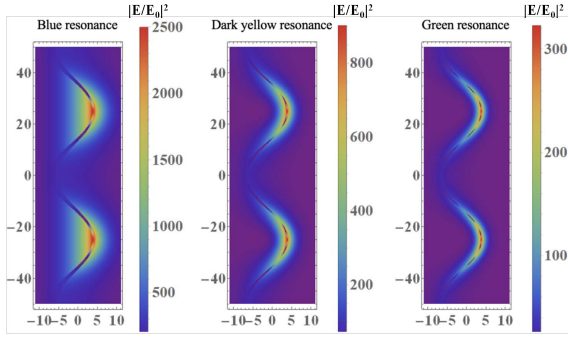


FIG. 4. Intensity of local electric field in a modulated silver film for the blue, dark yellow, and green resonances displayed in Figure 3b, where the period is $L = 50 \text{ nm}$, modulation amplitude is $h = 11 \text{ nm}$, silver permittivity at $\lambda = 785 \text{ nm}$ is $\varepsilon_m = -30 + 0.4i$, permittivity of dielectric substrate is $\varepsilon_d = 2$, and permittivity of front space $\varepsilon_1 = 1$.

same than those described in Figures 3b and 4 ($\varepsilon_1 = 1$, $\varepsilon_d = 2$, i.e., the refractive index of the photoresist is $n = 1.41$). The simulations are done in COMSOL environment. The Maxwell equations are solved by the finite element method (FEM). We demonstrate the enhance-

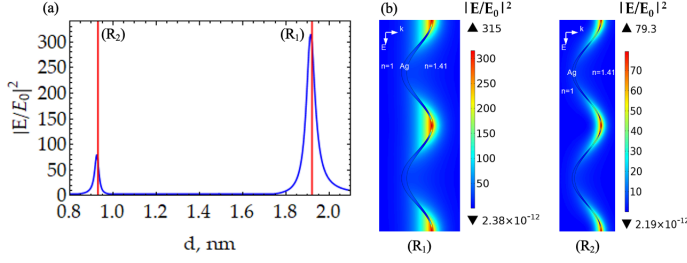


FIG. 5. (a) Electric field intensity for different thicknesses d of the silver film (illumination under normal incidence, with the following parameters: $L = 50 \text{ nm}$ and $h = 11 \text{ nm}$). The red vertical lines indicate resonance thicknesses obtained from analytical theory. (b) Distributions of the electric field intensity corresponding to two resonances (R_1) and (R_2) displayed in figure 5a.

ment of the electric field $|E/E_0|^2$ in the modulated thin metal film with period $L = 50 \text{ nm}$ and amplitude of the modulation $h = 11 \text{ nm}$ (see Figure 5). It can be seen that positions of the analytical and numerical resonances are in a good agreement. The distribution of the electric field for two resonances shown in Figure 5a are displayed in Figure 5b. Computer simulations are in agreement with analytical theory (see the blue and dark yellow resonances in figure 4). We also simulate the resonant enhancement of the electric field for a modulated metal film whose parameters correspond to the experiment discussed below (see Figure 6). Figure 6a,b show the distribution of the electric field intensity calculated with the result of Eq. (24) of the analytical theory, and computer simulations, respectively. Resonances are due to the excitation of dipolar and multipolar plasmons in

the modulated metal film. The electric field distribution in dipolar and multipolar plasmons is in qualitative agreement with analytical theory [see the resonances: (I), (II), and (III) displayed in figure 6a,b]. The field distribution in the resonance (IV) in Figure 6b,c differs from all other resonances. The electric field expands from the metal surface on the distance comparable with the wavelength and period of the modulation. We speculate that in this case the plasmon resonance hybridizes with plasmon propagating over the modulated metal surface (see, e.g., [40]). The hybridization could be the subject for the further consideration. In summary, we present

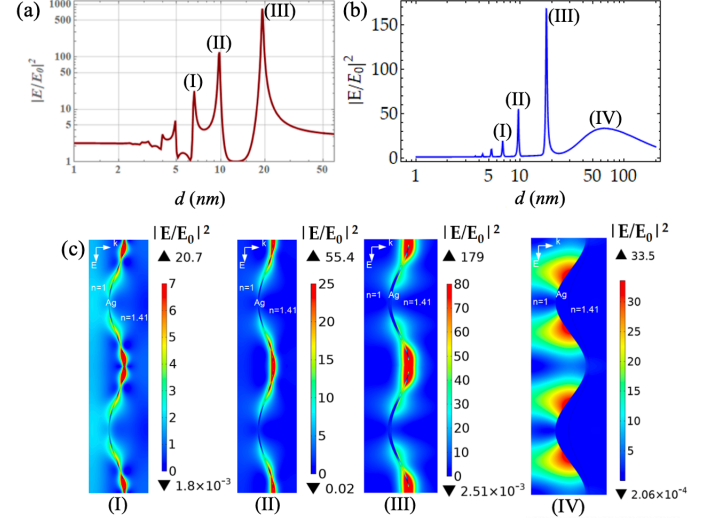


FIG. 6. Intensity of electric field for different thicknesses of silver film d with the following parameters: period $L = 750 \text{ nm}$ and amplitude of the modulation $h = 100 \text{ nm}$ (illumination at $\lambda = 785 \text{ nm}$, under normal incidence), calculated by using (a) the result of Eq. (24) and (b) computer simulations. (c) Computer simulation of distribution of local electric field corresponding to resonances: (I), (II), (III) and (IV) displayed in figure Fig. 6b.

the analytical theory of plasmons excited in a modulated metal film deposited on a dielectric substrate. Computer simulations and results given by the analytical theory are in a good agreement. The resonance conditions are found as a function of the metal permittivity, the modulation and the thickness of the film. When the grating is excited by the incident light, the surface electric field is much enhanced. The quasistatic theory qualitatively described the field enhancement even in the case $kL \approx 1$, since the field is concentrated in the nanograting whose thickness and modulation are much smaller than λ . The size of a plasmon maxima l_p is on the order of the film modulation $l_p \approx h$ (see Figs. 4, 5, 6). The radiation loss, which is proportional to $l_p dk^2$ remains to be less than one. For example, for silver film with parameters $h = 100 \text{ nm}$, $d = 20 \text{ nm}$ and $\lambda = 785 \text{ nm}$ (see Fig. 6), $l_p dk^2 \approx 0.1 < 1$. The positions of the plasmon resonances from computer simulations are almost coincide with re-

sults of Eq. (23). The resonance enhancement of the electric field obtained in computer simulations is very large. Yet, the computer results are few times smaller than results of the quasistatic Eq. (24). The discrepancy is due to the radiation loss that can be taken into account by using a perturbation theory. Yet, we do not expect qualitative difference between the quasistatic approximation and exact result while plasmons are localized like in resonances (I) - (III) (Figure 6). The developed analytical theory can be used for the design of new SERS substrates and other optical sensors. The theory can be extended to multilayered metal-dielectric films.

III. EXPERIMENTAL INVESTIGATION OF HOLOGRAPHIC METASURFACES

A. Fabrication process

The metasurfaces are fabricated by the following steps. As a first step $1.5 - 1.9 \mu\text{m}$ recording layer of positive photoresist (Microposit S1800) is deposited by spin-coating on the silicon wafer. Then, fifteen areas of two-dimensional modulated films ($1.5 \times 1.5 \text{ cm}^2$) are formed by holographic lithography technique. The principle scheme of recording setup employs a phase-modulator HED-6001 Monochrome LCOS, and an ultraviolet laser ($\lambda = 405 \text{ nm}$) (see Figure 7a). Exposure dose is varied from 4.1 to $8.5 \mu\text{J}/\text{cm}^2$. The angle between interfering light waves is around 49° . Next, the resist is developed in Microposit 303A developer. Afterwards, two successive depositions of a 80-nm SiO_2 layer and a 60-nm silver layer are realized by electron beam evaporation. The metasurfaces with period from 720 nm to 770 nm and modulation amplitude from 8 nm to 30 nm are fabricated (see Figure 7b). The principle scheme of the metasurface morphology is shown in Figure 7c. The morphology of the fabricated metasurfaces is measured with a scanning electron microscopy (SEM, JEOL), and SEM images of these metasurfaces are shown in Figure 7d,e. Finally, modulation amplitude measurements are made with an atomic force microscopy (AFM; Solver Pro NT-MDT) for different exposure doses (see Figure 7f).

B. Deposition of 4-Mercaptophenylboronic Acid for SERS

In order to study the sensitivity of the holographic metasurfaces, we employed molecules of 4-mercaptophenylboronic acid (4-mPBA), which are small molecules (thickness of a 4-mPBA monolayer is around 0.8 nm [65]). We have chosen the boronic acid, which is a specific substance because the boron group covalently binds diols and forms a boron ester. Therefore, boronic acid is considered as a specific agent for sugars and their fragments. There is a strong covalent fixation of this acid on the surface of silver due to the thiol group

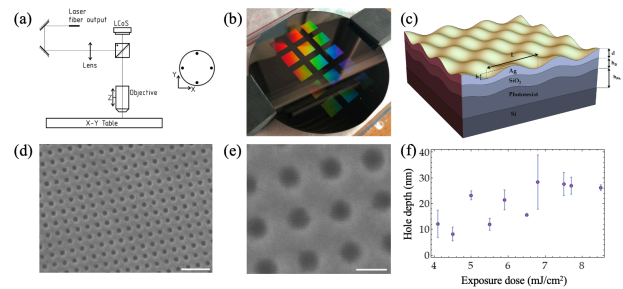


FIG. 7. (a) Principle scheme of the recording setup. (b) Photo of 4-inch wafer where holographic metasurfaces are fabricated. (c) Principle scheme of the metasurface design with the following parameters: period is $L = 720 - 770 \text{ nm}$, modulation amplitude is $h = 8 - 30 \text{ nm}$, silver layer thickness is $d = 60 \text{ nm}$, thickness of SiO_2 is $h_{\text{Si}} = 80 \text{ nm}$, photoresist thickness is $h_{\text{Ph}} = 1.5 - 1.9 \mu\text{m}$. SEM images of the metasurfaces (Period $L \approx 760 \text{ nm}$, and film modulation $h \approx 30 \text{ nm}$) with a scale bar of $2 \mu\text{m}$ for (d) and 500 nm for (e). (f) Hole depth versus exposure dose (depth measured by AFM).

(-SH). The analyzed molecules are covalently bound to the silver, thereby increasing the probability of the location of molecules in the region of generation of giant electromagnetic fields. In addition, we prepared solutions of 4-mPBA in ethanol with concentrations varying from $2.3 \times 10^{-8} \text{ M}$ to $2.3 \times 10^{-3} \text{ M}$. Then, for SERS experiments, an aliquot of each 4-mPBA solution was applied onto holographic metasurface and then dried at room temperature.

C. Optical Characterization

For characterizing the optical properties of metasurfaces, the reflectance spectra have been recorded by using a spectroscopic ellipsometer SE 850 DUV (Sentech, Germany). For the SERS measurements, a Raman spectrometer InnoRam (BWTEK, USA) with an excitation wavelength of 785 nm and a spectral resolution of 4 cm^{-1} was employed. The acquisition time and the laser power have been set at 1 s and 3.84 mW , respectively. A microscope objective ($\times 50$, $\text{NA} = 0.8$) was used in order to focus the laser beam on the metasurface, and the Raman signal of the 4-mPBA molecules immobilized on metasurface was detected by this same objective in a backscattering configuration.

IV. RESULTS AND DISCUSSION

A. Optical properties of holographic metasurfaces

To determine the macroscopic optical properties of metasurfaces, the angular reflectance spectrum is measured by ellipsometry in the range from 20° to 70° . The reflectance spectrum is measured for two polarizations:

R_p for p -polarization of the incident light and R_s for s -polarization of the incident light. The measured reflectance spectra for R_p and R_s show deep gaps with a complex behavior versus period and angle (see Figure 8). Raman instruments are usually attached to microscopes,

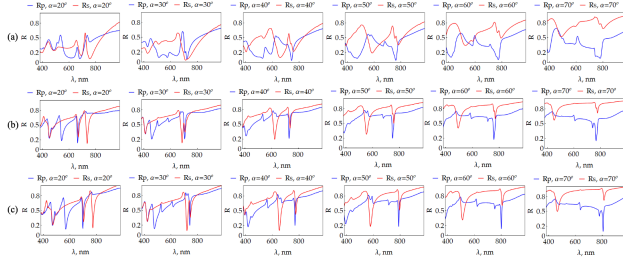


FIG. 8. Experimental angular reflectance spectra from the metasurface for different angles of the incident light and with the following structure parameters: (a) $L = 720$ nm, depth $h \approx 30$ nm; (b) $L = 720$ nm, depth $h \approx 20$ nm; (c) $L = 770$ nm, depth $h \approx 18$ nm.

where the excitation and the inelastically scattered light are delivered. The light is collected from the sample through the same objective in a backscattering geometry. The objective is characterized by a numerical aperture (NA) equal to 0.8 in our case. This means that the cone angle is equal to $2\alpha = \arcsin(NA) = 106^\circ$. So, we have to take into account all the rays of the incident light at angles α from 0° to 53° degrees. The focal length f is related to the lens diameter by the ratio $(D/2f) = \tan \alpha$ (D - lens diameter). We find the average reflection in the approximation of the geometric optics by integrating the reflection over the basis of the cone of the incidence. The principle scheme of the polarized light collected by the lens is displayed in Figure 9a. The average reflection is expressed as follows:

$$R_{average} = 2 \left(\frac{1}{NA^2} - 1 \right) \int_0^{\alpha_{max}} \frac{\sin \alpha}{\cos \alpha^3} R(\alpha) d\alpha \quad (26)$$

where $\alpha_{max} = \arcsin(NA)$. In addition, each ray has a transverse and longitudinal field component, so we average R_p and R_s . The resulting average reflection is displayed in Figure 9b. We observe minima on the spectral range from 400 nm to 800 nm and more specifically close to the excitation wavelength of 785 nm. We assume that these minima in the reflectance spectrum correspond to plasmon resonances. These plasmonic resonances (close to the excitation wavelength of 785 nm) will permit the enhancement the Raman signal of 4-mPBA molecules.

B. SERS detection of 4-mercaptophenylboronic acid molecules

For all the SERS experiments, a modulated silver metasurface with a period $L = 760$ nm, $h = 30$ nm is used. This metasurface has the maximum available modulation depth $h = 30$ nm. With a higher modulation

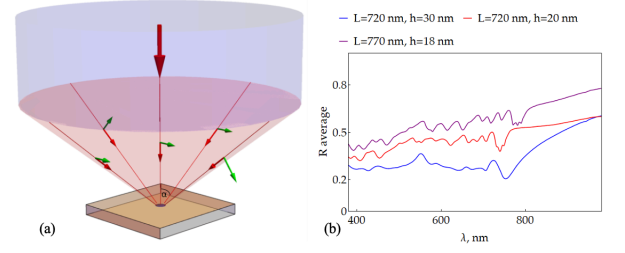


FIG. 9. (a) Schematic illustration of the polarized light impinging to the sample by the lens. The red and green arrows show the directions of the wave-vector and the electric field, respectively. (b) Average experimental reflectance spectra from modulated silver film (metasurface), the reflectance is averaged over the light cone, which is focused by the Raman microscope on the sample.

depth, the number of electromagnetic modes increases. Thus, this modulation allows obtaining deep minima in the reflectance spectrum close to the excitation wavelength of 785 nm (see figure 9b). Then, to evaluate the sensitivity of these metasurfaces, 4-mPBA molecules are grafted onto them by using the functionalization protocol described in section 3.2. Next, the SERS spectra have been recorded at the excitation wavelength of 785 nm. Figure 10 shows the SERS spectra of 4-mPBA molecules on metasurfaces obtained for each concentration varying from 2.3×10^{-8} M to 2.3×10^{-3} M. From the SERS spectrum obtained for the concentration of 2.3 mM depicted in Figure 10, seven characteristic Raman peaks of 4-mPBA molecules are well-distinguished [59, 66, 67]. The Raman peaks at 420 cm^{-1} , 693 cm^{-1} and 1072 cm^{-1} correspond to the C-C-C in-plane bending mode coupled with C-S stretching mode (called respectively: β_{CCC} and ν_{CS}). Then, the peak at 480 cm^{-1} corresponds to the C-C-C out-of-plane bending mode coupled to O-B-O in-plane bending mode (called respectively: γ_{CCC} and β_{OBO}). The Raman peaks at 1000 cm^{-1} and 1030 cm^{-1} correspond, respectively, to the C-C-C in-plane bending mode (called β_{CCC}) and the C-H in-plane bending mode (called β_{CH}). Finally, the Raman peak at 1580 cm^{-1} corresponds to the C-C stretching vibrational modes (called ν_{CC}). For determining the detection limit, we have chosen the most intense Raman peak, which is located at 1072 cm^{-1} , and a detection limit of 230 nM was achieved for the sensing of 4-mPBA molecules (see Figure 10 where the blue zone corresponds to the zone of the $3 \times$ noise level for the last curve) with a signal-to-noise ratio > 3 .

In addition, the distribution of Raman hotspots generated by periodic holes (grid) repeats the morphology of the surface, which is shown on the optical image displayed in Figure 7. Therefore, we can see the SERS effect distributed uniformly over the entire metasurface. The pattern of the Raman signal in Figure 11 repeats the periodic structure of the modulated film. Therefore, the maxima of the Raman signal repeat the maxima of the plasmon field $I(x, y)$. One could suggest that the SERS is a local effect, namely, $G(x, y) \propto I(x, y)^2$. Investigation

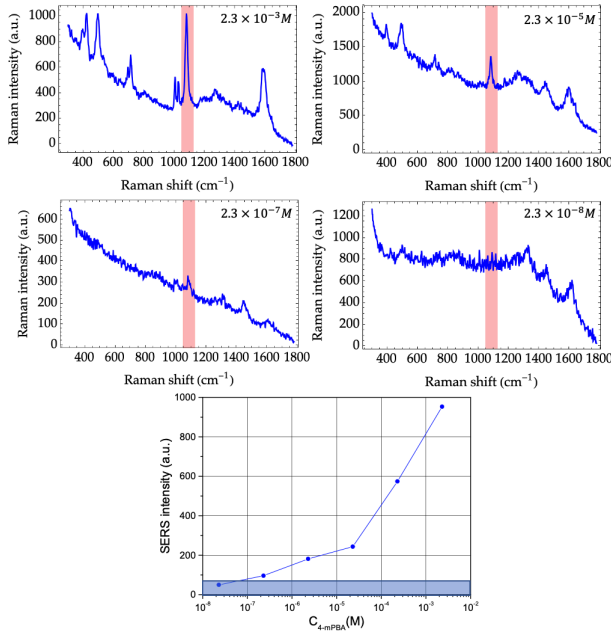


FIG. 10. SERS spectra of 4-mPBA molecules recorded on the metasurface for the concentrations of 2.3×10^{-3} M, 2.3×10^{-5} M, 2.3×10^{-7} M and 2.3×10^{-8} M. At the bottom of the figure, graph of SERS intensity versus 4-mPBA concentration, where the blue zone corresponds to the zone of the $3 \times$ noise level.

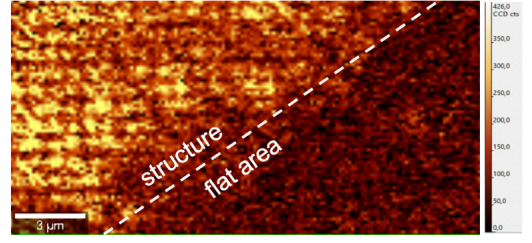


FIG. 11. Optical image of the intensity distribution for the Raman bands 1060–1100 cm^{-1} .

of the modulated metal film with progressively smaller period L can confirm locality of SERS effect.

V. CONCLUSION

In this paper, we presented the low-cost fabrication and the study of a resonant metasurface consisting of a periodically modulated metal film that exhibits an anomalous optical response due to the excitation of localized surface plasmons. The distribution of the enhanced electric field generated by the film modulation has repeated the surface morphology, and this distribution was uniform over this entire surface. The holographic metasurface allowed achieving a detection limit of 230 nM for the 4-mPBA molecules serving here as a proof-of-concept of SERS sensing. Thus, the low-cost and easy-made holographic SERS metasurfaces modified with 4-mPBA molecules can be used for quantitative biosensing of glycosylated proteins and sugars. Moreover, the analytical theory can allow the design and the optimization of various plasmonic sensors.

VI. FUNDING

This work was supported by the Russian Foundation for Basic Research (Grant No. 20-21-00080). The Raman measurements were supported by the Russian Science Foundation (Grant No. 21-79-30048).

-
- [1] B. Sharma, R. R. Frontiera, A. -I. Henry, E. Ringe, and R. P. Van Duyne, *Mater. Today* **15**, 16 (2012).
 - [2] J. Yan, X. Han, J. He, L. Kang, B. Zhang, Y. Du, H. Zhao, C. Dong, H. -L. Wang, and P. Xu, *ACS Appl. Mater. Interfaces* **4**, 2752 (2012).
 - [3] G. Bodelon, V. Montes-Garcia, V. Lopez-Puente, E. H. Hill, C. Hamon, M. N. Sanz-Ortiz, S. Rodal-Cedeira, C. Costas, S. Celiksoy, I. Perez-Juste, L. Scarabelli, A. La Porta, J. Perez-Juste, I. Pastoriza-Santos and L. M. Liz-Marzan, *Nat. Mater.* **15**, 1203 (2016).
 - [4] A. K. Sarychev, A. Ivanov, A. Lagarkov, and G. Barbillon, *Materials* **12**, 103 (2019).
 - [5] G. Barbillon, A. Ivanov, and A. K. Sarychev, *Symmetry* **12**, 896 (2020).
 - [6] J. Henzie, J. Lee, M. H. Lee, W. Hasan, and T. W. Odom, *Annu. Rev. Phys. Chem.* **60**, 147 (2009).
 - [7] Q. Yu, P. Guan, D. Qin, G. Golden, and P. M. Wallace, *Nano Lett.* **8**, 1923 (2008).
 - [8] A. -C. Faure, G. Barbillon, M. Ou, G. Ledoux, O. Tillement, S. Roux, D. Fabregue, A. Descamps, J. -L. Bijeon, C. A. Marquette, C. Bilottey, C. Jamois, T. Benyatou, and P. Perriat, *Nanotechnology* **19**, 485103 (2008).
 - [9] V. R. Manfrinato, F. E. Camino, A. Stein, L. H. Zhang, M. Lu, E. A. Stach, and C. T. Black, *Adv. Funct. Mater.* **29**, 1903429 (2019).

- [10] G. Barbillon, A. Ivanov, and A. K. Sarychev, *Nanomaterials* **11**, 1521 (2021).
- [11] P. Zhang, S. Yang, L. Wang, J. Zhao, Z. Zhu, B. Liu, J. Zhong, and X. Sun, *Nanotechnology* **25**, 245301 (2014).
- [12] G. Barbillon, J. -L. Bijeon, G. L  rondel, J. Plain, and P. Royer, *Surf. Sci.* **602**, L119 (2008).
- [13] A. Dhawan, A. Duval, M. Nakkach, G. Barbillon, J. Moreau, M. Canva, and T. Vo-Dinh, *Nanotechnology* **22**, 165301 (2011).
- [14] N. Guisbert Quilis, M. Lequeux, P. Venugopalan, I. Khan, W. Knoll, S. Boujday, M. Lamy de la Chapelle, and J. Dostalek, *Nanoscale* **10**, 10268 (2018).
- [15] J. S. Hwang and M. Yang, *Sensors* **18**, 4076 (2018).
- [16] T. Gong, Y. Luo, C. Zhao, W. Yue, J. Zhang, Y. Zhu, M. Pu, Z. Zhuojun, C. Wang, and X. Luo, *OSA Continuum* **2**, 582 (2019).
- [17] T. Ding, D. O. Sigle, L. O. Herrmann, D. Wolverson, and J. J. Baumberg, *ACS Appl. Mater. Interfaces* **6**, 17358 (2014).
- [18] C. Farcau, D. Marconi, A. Colnita, I. Brezestean, and L. Barbu-Tudoran, *Nanomaterials* **9**, 1519 (2019).
- [19] S. Goetz, M. Bauch, T. Dimopoulos, and S. Trassi, *Nanoscale Adv.* **2**, 869 (2020).
- [20] J. F. Masson, K. F. Gibson, and A. Provencher-Girard, *J. Phys. Chem. C* **114**, 22406 (2010).
- [21] M. Bechelany, P. Brodard, J. Elias, A. Brioude, J. Michler, and L. Philippe, *Langmuir* **26**, 14364 (2010).
- [22] G. Barbillon, T. Noblet, B. Busson, A. Tadjeddine, and C. Humbert, *J. Mater. Sci.* **53**, 4554 (2018).
- [23] Y. F. C. Chau, K. H. Chen, H. P. Chiang, C. M. Lim, H. J. Huang, C. H. Lai, N. T. R. N. Kumara, *Nanomaterials* **9**, 1691 (2019).
- [24] A. I. Kuznetsov, R. Kiyani, and B. N. Chichkov, *Opt. Express* **18**, 21198 (2010).
- [25] A. Lagarkov, I. Boginskaya, I. Bykov, I. Budashov, A. Ivanov, I. Kurochkin, I. Ryzhikov, I. Rodionov, M. Sedova, A. Zverev, and A. K. Sarychev, *Opt. Express* **25**, 17021 (2017).
- [26] G. Barbillon, A. Ivanov, and A. K. Sarychev, *Nanomaterials* **9**, 1588 (2019).
- [27] Q. Zhou, Y. Liu, Y. He, Z. Zhang, and Y. Zhao, *Appl. Phys. Lett.* **97**, 121902 (2010).
- [28] K. Seal, A. K. Sarychev, H. Noh, D. A. Genov, A. Yamilov, V. M. Shalaev, Z. C. Ying, and H. Cao, *Phys. Rev. Lett.* **947**, 226101 (2005).
- [29] D. A. Genov, A. K. Sarychev, V. M. Shalaev, and A. Wei, *Nano Lett.* **4**, 153 (2004).
- [30] A. Ivanov, A. Shalygin, V. Lebedev, P. Vorobev, S. Vergiles, and A. K. Sarychev, *Appl. Phys. A* **107**, 17 (2012).
- [31] L. L. Frumin, A. V. Nemykin, S. V. Perminov, and D. A. Shapiro, *J. Opt.* **15**, 085002 (2013).
- [32] Z. -Q. Liu, G. Q. Liu, X. S. Liu, K. Huang, Y. -H. Chen, Y. Hu, and G. -I. Fu, *Plasmonics* **8**, 1285 (2013).
- [33] G. -Q. Liu, Y. Hu, Z. -Q. Liu, Y. -H. Chen, Z. -J. Cai, X. -N. Zhang, and K. Huang, *Phys. Chem. Lett.* **16**, 4320 (2014).
- [34] G. -Q. Liu, Y. Hu, Z. -Q. Liu, Z. -J. Cai, X. -N. Zhang, Y. -H. Chen, and K. Huang, *Opt. Commun.* **316**, 111 (2014).
- [35] I. L. Rasskazov, V. A. Markel, and S. V. Karpov, *Opt. Spectrosc.* **115**, 666 (2013).
- [36] A K Sarychev, A V Ivanov, and G Barbillon, *QUANTUM ELECTRON* **51**, 79 (2021).
- [37] A. Demetriadou, J. M. Hamm, Y. Luo, J. B. Pendry, J. J. Baumberg, O. Hess, *ACS Photonics* **4**, 2410 (2010).
- [38] F. Ding, Y. Yang, R. A. Deshpande, and S. I. Bozhevolnyi, *Nanophotonics*, **7**, 1129 (2018).
- [39] L. A. Vainshtein, *Open Resonators and Open Waveguides*; Golem Press: Boulder, Colo., 1969.
- [40] A. M. Dykhne, A. K. Sarychev, and V. M. Shalaev, *Phys. Rev. B* **67**, 195402 (2003).
- [41] X. Deng, G. B. Braun, S. Liu, P. F. Sciortino, B. Koefler, T. Tomblar, and M. Moskovits, *Nano Lett.* **10**, 1780 (2010).
- [42] A. N. Lagarkov, I. Budashov, V. Chistyayev, A. Ezhov, A. Fedyanin, A. Ivanov, I. Kurochkin, S. Kosolobov, A. Latyshev, D. Nasimov, I. Ryzhikov, M. Shcherbakov, A. Vaskin, and A. K. Sarychev, *Opt. Express* **24**, 7133 (2016).
- [43] K. N. Kanipe, P. P. F. Chidester, G. D. Stucky, and M. Moskovits, *ACS Nano* **10**, 7566 (2016).
- [44] J. B. Pendry, D. Schurig, and D. R. Smith, *Science* **312**, 1780 (2006).
- [45] U. Leonhardt, *Science* **312**, 1777 (2006).
- [46] M. Kraft, Y. Luo, S. A. Maier, and J. B. Pendry, *Phys. Rev. X*, **5**, 031029 (2015).
- [47] P. A. Huidobro; Y. H. Chang, M. Kraft, and J. B. Pendry *Phys. Rev. B* **95**, 155401 (2017).
- [48] J. B. Pendry, P. A. Huidobro, Y. Luo, E. Galiffi, *Science* **358**, 915–917 (2017).
- [49] J. B. Pendry, P. A. Huidobro, and K. Ding, *Phys. Rev. B* **99**, 085408 (2019).
- [50] E. Galiffi, J. B. Pendry, and P. A. Huidobro, *ACS Nano* **12**, 1006-1013 (2018).
- [51] F. Yang, P. A. Huidobro, and J. B. Pendry, *Phys. Rev. B* **98**, 125409 (2018).
- [52] F. Yang, E. Galiffi, P. A. Huidobro, and J. B. Pendry, *Phys. Rev. B* **101**, 075434 (2020).
- [53] F. Yang, P. A. Huidobro, and J. B. Pendry, *Laser Photonics Rev.* **14**, 2000055 (2020).
- [54] L. Lu, E. Galiffi, K. Ding, T. Dong, X. Ma, and J. B. Pendry, *ACS Photonics* **7**, 951 (2020).
- [55] L. Dong, X. Yang, C. Zhang, B. Cerjan, L. Zhou, M. L. Tseng, Y. Zhang, A. Alabastri, P. Nordlander, N. J. Halas, *Nano Lett.* **17**, 5678 (2017).
- [56] Kneipp, J. *ACS Nano* **11**, 1136 (2017).
- [57] Y. Hu, H. Cheng, X. Zhao, J. Wu, F. Muhammad, S. Lin, J. He, L. Zhou, C. Zhang, Y. Deng, P. Wang, Z. Zhou, S. Nie, and H. Wei, *ACS Nano* **11**, 5558 (2017).
- [58] C. Andreou, V. Neuschmelting, D. -F. Tschaharganeh, C. -H. Huang, A. Oseledchyk, P. Iacono, H. Karabeber, R. R. Colen, L. Mannelli, S. W. Lowe, and M. F. Kircher, *ACS Nano* **10**, 5015 (2016).
- [59] N. L. Nechaeva, I. A. Boginskaya, A. V. Ivanov, A. K. Sarychev, A. V. Eremenko, I. A. Ryzhikov, A. N. Lagarkov, and I. N. Kurochkin, *Anal. Chim. Acta* **1100**, 250 (2020).
- [60] H. Chon, S. Lee, S. -Y. Yoon, E. K. Lee, S. -I. Chang, and J. Choo, *Chem. Commun.* **50**, 1058 (2014).
- [61] P. B. Johnson and R. W. Christy, *Phys. Rev. B* **6**, 4370 (1972).
- [62] L. D. Landau, E. M. Lifshitz, L. P. Pitaevskii, "Electrodynamics of Continuous Media," Vol. 8 (2nd ed.) (1984).
- [63] S. Mariazzi, P. Bettotti, S. Larcheri, L. Toniutti, and R. S. Brusa, *Phys. Rev. B* **81**, 235418 (2010).
- [64] F. Brouers, S. Blacher, A. N. Lagarkov, A. K. Sarychev, P. Gadenne, and V. M. Shalaev, *Phys. Rev. B* **55**, 13234

- (1997).
- [65] D. Barriet, C. M. Yam, O. E. Shmakova, A. C. Jamison, T. Randall Lee, *Langmuir* **23**, 8866 (2007).
- [66] H. Su, Y. Wang, Z. Yu, Y. Liu, X. Zhang, X. Wang, H. Sui, C. Sun, B. Zhao, *Spectrochim. Acta Part A Mol. Biomol. Spectrosc.* **185**, 336 (2017).
- [67] F. Sun, T. Bai, L. Zhang, J. -R. Ella-Menye, S. Liu, A. K. Nowinski, S. Jiang, Q. Yu *Anal. Chem.* **86**, 2387 (2014).